Chapter 1
Failure Mechanisms

Plastics Failure Due to Oxidative Degradation in Processing and Service

Myer Ezrin, Amanda Zepke, John Helwig, Gary Lavigne and Mark Dudley
University of Connecticut, Institute of Materials Science, Storrs, CT 06269-3136, USA

INTRODUCTION

People cannot live without oxygen and water. But these are deadly enemies of polymers, both in processing of plastics formulations and in service. Water is a problem mainly for condensation polymers which degrade by hydrolysis. In this paper the focus is on oxidative degradation.

Oxygen degrades polymers to lower molecular weight (MW) by reacting with polymer free radicals to form peroxy free radicals (ROO•) and hydroperoxides (ROOH). Free radicals have an unshared electron and react in any way they can to restore the atom or molecule to a balanced structure. Often that leads to chain scission. As MW goes down most polymer properties suffer. As little as 5-10% reduction in MW may cause failure. Avoiding contact with oxygen and using an antioxidant (AO) as a free radical scavenger are means of preventing degradation.

The high temperature required to process plastics is the major cause of degradation in injection molding, extrusion, blow molding, etc. High temperature is needed to fuse polymers and to reduce melt viscosity to a level that the machines can handle. Mechanical shear of the melt and the presence of oxygen, even in small amounts, are major factors in degradation due to processing. The chain carbon atoms attached to a branch, such as methyl group (CH_3), tend to split off a hydrogen atom, creating a free radical at a tertiary carbon atom.

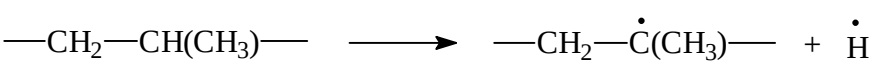

Very little oxygen is needed to react with free radicals during processing. Polymer suppliers usually have very little AO in the resin as sold to processors. Unless additional AO is added, polymer is likely to degrade in process. Polyolefins, which have only carbon-carbon chain bonds (PE, PP, EP and other copolymers) are particularly susceptible to oxidative degradation, in service as well as in processing. Even if additional AO is added, severe processing conditions (high temperature, high shear, long residence time in the barrel), use of regrind, etc. may deplete most of the AO, leaving too little to withstand conditions in service.

Even in moderate service conditions, such as a PE eyewash squeeze bottle on a laboratory wall, oxidative degradation can lead to failure in long term applications. Such a PE bottle, which had been on a laboratory wall for 15-20 years, cracked when tested in a safety inspection. Here, too, additional AO is needed to survive many years of service.

A complicating factor in processing is formulations containing peroxides to crosslink the polymer. Peroxide causes crosslinking by decomposing to free radicals ($ROOR \rightarrow 2R\dot{O}$). The high content of peroxy free radicals formed abruptly reacts with the polymer to cause crosslinking. These free radicals may react with the AO, leaving the system without enough AO for the polymer to survive processing and service. The AO system must be chosen accordingly.

Commonly used methods of analysis to determine if failure is due to oxidative degradation are differential scanning calorimetry (DSC) for oxidative induction time (OIT), (ASTM D3895) or oxidative induction temperature (ASTM D3350). Infrared spectroscopy (IR) may detect bound oxygen as carbonyl (C=O), which forms increasingly as AO becomes exhausted. A third method is change in MW measured as an increase in melt flow rate (MFR), (ASTM D1238). This is a very practical method because it relates directly to MW, i.e., a small reduction in MW gives a large increase in MFR. The applicable relationship is $n=KM^{3.4}$. Gel permeation chromatography (GPC) is also useful for monitoring MW changes in processing or service.

The DSC methods require about an hour or less, after establishing test conditions, and are most useful for comparing materials, e.g., before and after processing, or after service. They are a practical method of determining the relative amount of AO remaining. When a sample's AO content is zero, oxidation exotherm starts very soon after oxygen is admitted into the DSC cell. Additional information on the DSC methods is given in the next section. IR is useful mainly to detect bound oxygen, which occurs when most or all of the AO has been depleted.

Examples are given below of failure due to oxidative degradation for (1) HDPE power cable jacket; (2) PE low voltage cable in a power plant control room; (3) PP rotors in a hot

water system; (4) EPDM hot water check valve; and (5) EVA (ethylene vinylacetate) hot melt adhesive degraded in a heated reservoir.

A recent case of PP failure in hot water heaters, most likely due to oxidative degradation, was reported in Consumer Reports, July 1999, p. 8. PP that replaced copper dip tubes brings cold water to the bottom of the heater. The PP has been disintegrating into small pieces and clogging pipes and other water delivery systems, and preventing normal operation of the hot water heater. Class action law suits have been filed in some states. Sixteen million heaters were made between 1993 and 1996 with PP dip tubes that may be defective.

EXPERIMENTAL METHODS

DSC - OXIDATIVE INDUCTION TIME AND OXIDATIVE INDUCTION TEMPERATURE

The OI time method requires selecting an isothermal temperature, first equilibrated in nitrogen, then changing to oxygen for the test. For PE and PP a common temperature is 200°C. The OI temperature method is much simpler, because a routine programmed temperature run is made using oxygen from the beginning. At some temperature an exotherm will be observed. OI time testing is critically dependent on selecting an appropriate isothermal temperature. Switching from nitrogen to oxygen may cause an upset in the baseline which could complicate interpretation of the result, i.e., did the exotherm start right away (zero minutes OIT) or is it at a higher value, which may be difficult to detect with some polymers.

The instrument used was a TA Instruments model 2920. The OI time method generally followed the guidelines of ASTM D3895. The isothermal temperature depends some-what on the material being tested, selected to give a time to exotherm of about 60 minutes for the most highly stabilized samples. Surface to volume ratio and sample weight affect the response to oxygen, affecting how readily and reproducibly the OI time is determined. The ASTM method calls for extrapolation of the initial part of the exotherm to the baseline (see DSC figures below). Extrapolation introduces some variability because not all samples in a group have similar exotherm slopes. A more realistic measure of OI time or OI temperature is the initial onset time or temperature (see DSC figures below). That is when the reaction with oxygen starts. Since the deflection off the baseline is often slight and gradual, a common or standard method needs to be used to detect the initial onset point because the temperature or time is not important by itself, only in comparison with similar samples with different process or service history. Uniform contact with the sample pan bottom is ideal. If OI time is required, an OI temperature run is helpful in selecting an appropriate isothermal temperature.

MOLECULAR WEIGHT-RELATED METHODS

Melt Flow Rate - ASTM D1238

If a sample no longer has AO, some degradation may occur in the MFR test at elevated temperature. That will give a value which is the sum of the change due to the sample's pretest history and its MFR test. This effect can be judged by running the test at various heating times in the barrel before extrusion. If MFR goes up as test time increases, degradation in the test is indicated.

Gel Permeation Chromatography

This method gives molecular weight distribution by passing a solution through columns of controlled pore size. The instrument used is a Waters 150C with THF solvent at 35°C and 1 ml/min. flow rate.

INFRARED SPECTROSCOPY

A Spectratech micro IR in the reflectance mode with a germanium crystal was used with a Nicolet Magna 560 FT/IR. While special attention is paid to the carbonyl (C=O) region at 1700-1750 cm^{-1}, the rest of the spectrum may indicate other changes due to processing or service.

EXPERIMENTAL RESULTS

HDPE POWER CABLE JACKET FRACTURE

Black HDPE jacket of a medium voltage power distribution cable experienced cracking in a certain pattern (Figure 1). The jacket was in contact with a copper foil wrap directly underneath it. Fracture occurred where the cable was wet in a manhole. Fracture lines were at the points where two layers of copper tape overlapped, putting pressure on the jacket along these lines. Fracture did not occur where jacket was dry. OI time extrapolated value at 199°C in oxygen was six minutes in areas where the copper and jacket had been wet. Using the initial onset temperature instead of the extrapolated value, OIT was zero. That is, all AO was depleted. The role of copper is important. In the wet state some copper is converted to the ionic form. Copper ion is a catalyst for reactions which result in oxidative degradation of PE. This failure was affected strongly by the contact of PE with copper in the ionic form due to water immersion. It also illustrates that an OIT

Figure 1. HDPE power cable jacket fractured by oxidative degradation due to water and copper in contact with jacket. Copper below jacket shows through cracks.

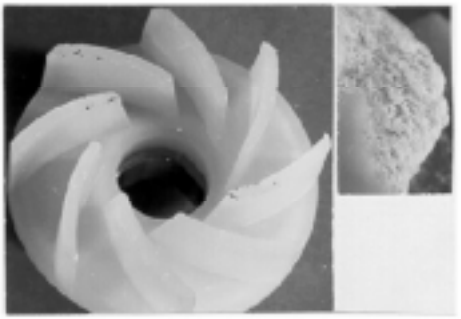

Figure 2. Unused PP rotor and closeup of a degraded fin of a used rotor.

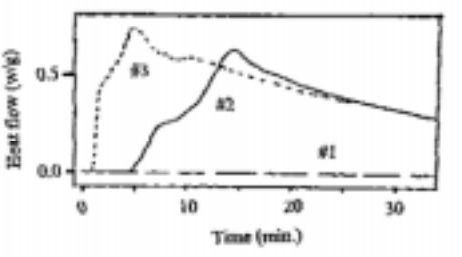

Figure 3. DSC-01 time at 200°C of #1 unmolded PP pellets (>50 min.); #2 unused molded rotor (4 min.); #3 rotor degraded in service (1 min.).

value of six minutes by extrapolation is really a value of zero at onset of the exotherm, for all practical purposes. The curvature of the cable meant that bending stress was also a factor in the jacket failure.

3.2 PE INSULATION IN A POWER PLANT CONTROL ROOM

Sections of 1/8" diameter PE insulation cracked, threatening the safety system of which the fractured PE was a part. Failure occurred in about 10 years particularly where wiring was near fluorescent lighting. At such locations OIT values were very low or zero minutes. In the worst cases of embrittlement, IR revealed carbonyl bond oxygen (C=O). Fluorescent lighting appears to have enough ultraviolet radiation to accelerate oxidative degradation. Areas well away from fluorescent lighting were relatively undegraded.

PP ROTORS IN A HOT WATER SYSTEM

In this case pellets, as-molded rotors, and degraded rotors were available to track the OIT values from “cradle to grave.” Degraded rotors in service for about a year experienced substantial degradation under service conditions of hot water, steam and air. Figure 2 shows a complete unused rotor, which measures about 2" in diameter. The photo includes a closeup of the degraded end of a fin of a used rotor. Figure 3 is the DSC-OIT thermogram of pellets, unused rotor as molded and a rotor degraded in service. Isothermal DSC temperature was 200°C. The OI time for pellets was >50 minutes; for as-molded rotors, time was 4 minutes; and degraded rotor was 1 minute. Time to purge the DSC cell with oxygen following equilibration in nitrogen was about 1 minute, so that the OI time of degraded rotor was practically zero.

The pellets were well stabilized (OIT >50 min.), so that an OIT value of 4 minutes for molded rotor indicates that most of the AO was consumed in processing. The type of service

Figure 4. EPDM hot water check valve molded on metal support. Surface is degraded and uneven; metal spring in center has broken through the degraded EPDM. Overall diameter is approx. 5/8 inch (20 mm).

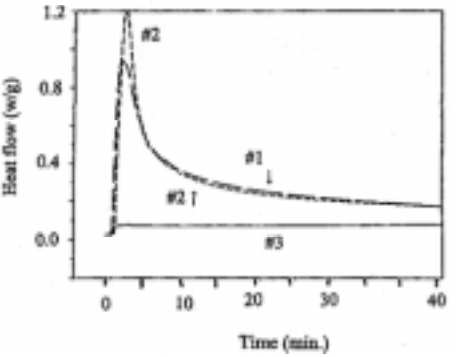

Figure 5. DSC-OI time at 210°C of EPDM valve - #1 failed in service (0 min.); #2 unused valve (0 min.); #3 a different EPDM that did not fail in service (>50 min.).

(hot water, air) readily consumed the remaining AO leaving the rotors very susceptible to degradation in service. It is possible that a different AO system might have provided better protection in processing and service.

EPDM EMBRITTLED IN HOT WATER CHECK VALVE

The part resembles a small mushroom with the EPDM covering a metal support (Figure 4). In the figure, the EPDM over the metal part in the center has fractured and been lost, leaving the metal exposed. A spring-loaded metal part in the center controls the valve. Failure in service was due to development of roughness of the EPDM surface and to the metal part breaking through the EPDM. OI time was performed at 210°C for valve material failed in service (#1), prior to service (#2), and for a different unused EPDM valve that had not failed in service (#3). Figure 5 shows that sample #3 had OIT of >50 minutes. The other two, made with a different EPDM formulation than #3, had OIT of zero.

OI temperature runs were made to see how the exotherm onset temperatures would compare to the OI times at 210°C. Figure 6 gives OI temperature runs for samples 1, 2 and 3. Representative initial onset and extrapolated values are indicated. Each test was done in duplicate, with remarkably good reproducibility. The greatest uncertainty is in the initial onset temperature for the good EPDM that did not fail (#3). The curve slopes up much more gradually than for #1 and #2. The OIT values are given in Table 1 for the initial onset and extrapolated values. They differentiate between #1 and #2, while OI time at 210°C gave values of zero for both. OI time tests at lower isothermal temperatures also gave very low values for #1 and #2. Thus OI temperature provided useful information more readily than OI time did, or would have required considerable effort to select the optimum temperature.

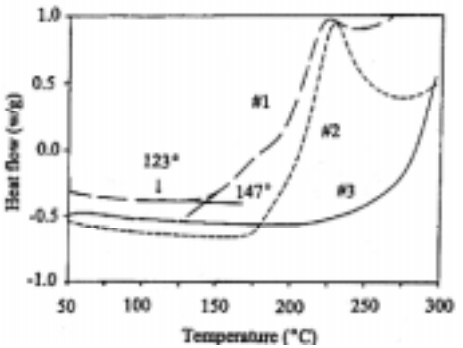

Figure 6. DSC-OI temperature of same samples as in Figure 5 - see Table 1 for initial onset and extrapolated OI temperatures. Values are shown for #1. 123° initial onset and 147° extrapolated.

Table 1. Oxidative induction temperature of EPDM

Sample	OIT, °C	
	Initial onset	Extrapolated
#1 - failed in service	122, 124 avg. 123	146, 147 147
#2 - same as #1 - unused	160, 159 avg. 160	175, 174 175
#3 - different EPDM unused	203, 167, 185 avg. 185	270, 270, 272 271

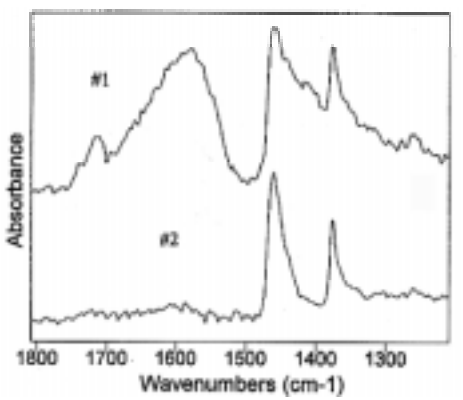

Figure 7. Micro IR reflectance spectra of EPDM valve - #1 degraded outer surface - bound oxygen at 1500-1800 cm^{-1} not present below surface; #2 inner bulk below degraded outer surface.

Table 1 indicates that the AO level as molded, before service, was enough to give an OI temperature initial onset value 37°C higher than after failure in service and 28°C higher by extrapolation. By comparison to #3, an earlier formulation that never failed in service, the newer material as made is much lower, 25° by initial onset and 96° by extrapolation. Clearly, the service condition requires an AO capability like that of #3. In the manufacture of the new valve, some AO is depleted in processing, and the amount remaining is not enough to protect the material in service (failure was in three months). Another possible contributor to the problem was that EPDM was crosslinked with dicumyl peroxide. As indicated above, free radicals from peroxide would have reacted with some of the AO.

Infrared spectroscopy (Figure 7) shows considerable bound oxygen in the surface of the failed material (upper curve), from 1500-1800 cm^{-1}, that is absent in the inner bulk of the same failed EPDM (lower curve). These spectra indicate that the oxidative degradation is limited to a very thin surface layer. However, embrittlement at the surface causes fracture

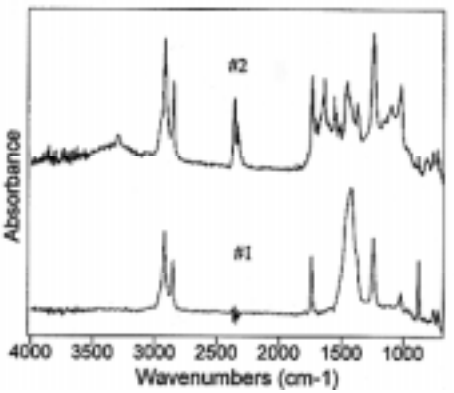

Figure 8. Micro IR reflectance spectra of EVA hot melt adhesive - #1 unfused pellets; #2 dark brown adhesive from heated reservoir.

to occur through the full thickness, following fracture initiation at the surface.

DEGRADED HOT MELT EVA ADHESIVE

The color after being in the hot reservoir was dark brown, compared to light tan pellets before heating. EVA (ethylene vinylacetate) can degrade by deacetylation, i.e., loss of acetic acid, with formation of a C=C double bond in the chain. This is independent of oxidative degradation, which occurs because of the ethylene units in the copolymer. OI temperature was performed to see to what extent oxidation is a factor also. For pellets initial onset temperature was 164° and by extrapolation 216°C. Dark material gave corresponding values of 148° and 206°C. These differences seem small relative to the very great difference in color. GPC for molecular weight distribution gave some reduction in MW of EVA, but also a considerably smaller GPC peak for degraded material. That corresponded to material which did not dissolve in hot toluene, whereas toluene did dissolve the pellets well. Toluene solutions were injected into the THF GPC solvent. IR spectra (Figure 8) of pellets and degraded material are different in ways that are not clear. The VA content has not changed much. The large peak near 1400 cm^{-1} is gone, as well as the small one near 900 cm^{-1}. These correspond to $CaCO_3$ filler, which appears to have reacted, possibly with acetic acid from vinylacetate. In this case oxidative degradation may have been partly responsible for the severe darkening, but other factors not readily understood may have been even more responsible.

SUMMARY

OI time and temperature are useful methods for deter-mining if oxidative degradation is the cause of polymer property loss due to processing and to service conditions. The methods are particularly attractive for polyolefins, which degrade to lower molecular weight oxidatively, and are very dependent on AO to minimize degradation. The OI temperature method is much simpler than OI time and in this study revealed differences between materials even better than OI time, in some cases. Together with other methods, such as GPC, melt flow rate and IR spectroscopy, failures due to oxidative and other causes of degradation can be determined. The result is a better understanding of the extent to which failure can be ascribed to processing, to service and to reactions other than oxidation.

Durability Study of Conductive Copper Traces Within Polyimide Based Substrates

Elena Martynenko, Wen Zhou and Alexander Chudnovsky
Fracture Mechanics and Materials Durability Laboratory, Civil and Materials Engineering Department, The University of Illinois at Chicago, 842 W. Taylor Street (M/C 246), Chicago, IL 60607, USA
Ron Li and Larry Poglitsch
Motorola Inc., Automotive and Industrial Electronics Group, 4000 Commercial Ave, Northbrook, IL 60062, USA

INTRODUCTION

Flexible circuits are widely used in various electronic packages. As the complexities of electronic packages grow, high reliability of assembled components is critical to maintain final product quality, especially in light of trends toward miniaturization and higher levels of integration. Electronic packages with FPC are used in every conceivable application from heart pacemakers, to automotive instrument clusters and to missile guidance systems. FPC failures may lead to serious consequences. A detailed understanding of why and how electronic packages fail greatly aids in the development of high-performance packaging with enhanced reliability. A variety of factors essential in the electrical, mechanical, and thermal design can contribute to the packaging failures. Properties of materials such as interconnection alloys, metal plating, laminates, adhesives, etc. can be a source of catastrophic failures if not properly understood and selected. Modern electronic systems in many applications experience severe vibrations and shocks. The failure appears to be due to submicroscopic cracks that grow into visible cracks and lead to a complete rupture without warning under repeated loading. Therefore, fatigue resistance is of major importance in reliability assessment of various electronic packaging.

The primary objective of this study is to determine high cycle fatigue resistance of certain flexible circuits. Various failure modes and mechanisms in electronic packages have been addressed in literature.[1-3] However, limited information has been presented on high cycle fatigue resistance of FPC. To the authors knowledge there was no reported study for a thermal fatigue testing of the material systems under consideration. The objective of this

study is to address the fatigue resistance as the function of temperature, displacement and frequency.

EXPERIMENTAL SETUP AND APPARATUS

To perform reliable high cycle fatigue testing, precise equipment is required. Specially designed experimental setup includes a sine servo controller, electrodynamic shaker, power amplifier, continuity monitor, temperature chamber with temperature control panel and sample fixture.

The sine servo controller is designed specifically for use in controlling wide band electrodynamic vibration shakers in sinusoidal testing applications. A wide operating frequency range makes it adaptable to almost any test situation from research and calibration to production testing. A 40 (75 peak) pound force electrodynamic shaker is designed for general-purpose vibration testing of small components and stress screening of electronic sub-assemblies. It provides a force output proportional to the input drive current from a power amplifier and consistently reproduces the waveform within the specified level and frequency bandwidth limits. The continuity monitor is a high frequency event detector that was used to determine the number of cycles to failure in each individual trace of the FPC samples.

MATERIALS AND EXPERIMENTAL PROCEDURES

FPC samples have been provided by *Motorola Inc*. All samples represent the single-sided conductor layer, double-access covered FPC (manufactured in accordance with IPC-FC-240 requirements) with a composite structure consisting of polyimide dielectric laminate and copper circuit traces, i.e., three layers – two dielectric layers and a single conductor.[4-7]

Flexible circuitry is typically a composite, of metal foil conductors, and a flexible dielectric substrate. The substrate insulates the conductors from each other and provides much of the circuit's mechanical strength. Plastic films, synthetic papers, and resin-impregnated fabrics have been used as dielectrics in flexible circuits, but polyimide and polyester films satisfy the widest spectrum of requirements.[8,9] The conductor material in FPC must survive processing and provide adequate electrical performance in the service environment. Conductor properties influence the flexural fatigue life of a flexible circuitry assembly. In many "static" applications, bending is limited to installation and servicing. In "dynamic" applications, the assembly is flexed or folded repeatedly during normal use. For dynamic applications, conductors should be of the minimum acceptable thickness and have high fatigue ductility. Conductors made of copper foil provide the best balance between conductivity, ease of processing, and cost.[10]

Three material systems *(*A, B and C) have been selected for our study. All of them consist of polymer matrix (polyimide) with embedded copper circuit traces. Dog-bone shape

samples have been prepared for fatigue studies. There are two asymmetric holes introduced for identification purpose to ensure consistent orientation. Sample thickness is 0.15 mm. Overall 16 samples of material system *A* have been tested. For each test condition at least 2 but in most cases 3 samples have been tested. This results in 16 to 24 data points for each loading condition.

To assure proper sample alignment during installation and testing, required bending as well as precise bonding at the selected domains special sample placement fixture has been designed. The 3M Com. adhesive film is used for bonding purposes. In our study flexes are bonded to the sample fixture via this pressure sensitive adhesive (PSA) film. Symmetrical bending is assured by bonding of the flexes to the fixture in specified domains. Specimen installation on the electrodynamic shaker is a complex procedure requiring special alignment steps and proper connection to continuity monitor.

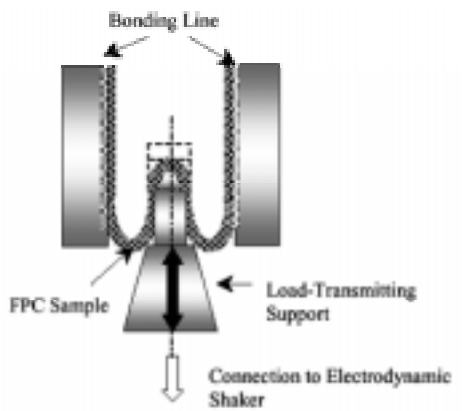

Figure 1. General schematic of load-transmitting support.

Displacement is transmitted through a vertical rod connected to the electrodynamic shaker. Displacement range is continuously detected by a sine servo controller and automatically adjusted via power amplifier according to the feedback reading of the accelerometer attached to the electrodynamic shaker. This experimental setup guarantees precise reading of displacement and acceleration ranges selected for testing conditions. General schematic of load-transmitting principle is shown in Figure 1.

A temperature chamber has been employed to perform thermal fatigue testing with precisely controlled temperature gradient. The following setup has been used on sine servo controller: output - manual; sweep – manual, continuous. Temperature in the range of 100±5°C has been selected for thermal fatigue studies. Frequencies of 60 Hz and 100 Hz have been selected for our study and displacement range from 1.27 mm to 3.81 mm has been utilized.

Initial and final count settings of the continuity monitor have been recorded for all eight traces in each sample and fatigue lifetime has been calculated based on those records. Each sample failure has been followed by a microscopical analysis via an optical microscope attached to a computerized image analyzing system. Digitized images of fracture surfaces of FPC circuit traces are provided in this study. Scanning Electron Microscopy (SEM) has been used in the analysis of failure modes of copper traces. Detailed fracture analysis

has been performed and failure modes have been established for each material system under investigation.

RESULTS AND DISCUSSIONS

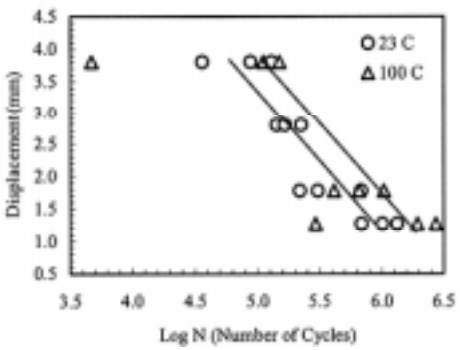

Figure 2. S-N (D-N) diagram for material system A.

Generally, the fatigue life is determined as the number of fatigue cycles required to produce a failure at a given stress level or under a given test conditions. In this study fatigue performance of certain material systems has been analyzed based on fatigue lifetime comparative analysis in addition to fracture analysis. High cycle fatigue testing has been performed under room (23 °C) and elevated (100 °C) temperatures. Two frequency "windows" have been selected: 60 Hz and 100 Hz. The following acceleration values have been selected 15 g, 23 g and 30 g. They are related to the following displacement values: 1.27, 1.78, 2.79 and 3.81 mm depending on frequency.

Fatigue resistance of chosen material systems has been analyzed as a function of temperature and frequency. The fatigue data for this system are reflected in Figure 2 where the number of cycles is given versus displacement, which can be directly related to stresses. Three data points are given for each displacement/loading condition: minimum, maximum and average. These data represent the average values of fatigue performance of particular traces of various samples tested under the same conditions. This representation provides the scatter of fatigue resistance of different traces subjected to the same testing conditions. As can be seen, higher displacements (stresses) significantly reduce fatigue lifetime of selected material system under room temperature. Similar trend is observed for elevated temperature (100°C).

Frequency effect can not be explicitly formulated in this study. However it is implicit in displacement effect, which corresponds to a particular acceleration under certain frequency.

To convert obtained data into conventional *S-N* curves, the Finite Element Analysis (FEA) has been performed. Dynamic stresses have been calculated based on FEA model. Shell elements with plasticity capability are used to simulate the flexible substrate. The bending profile of the substrate is measured from actual bending results. The flexible substrate is bonded to a rigid plate through pressure sensitive adhesive (PSA). The two rigid plates are fixed. The thin substrate is subject to displacement load along its symmetric plane. The finite element model is shown in Figure 3.

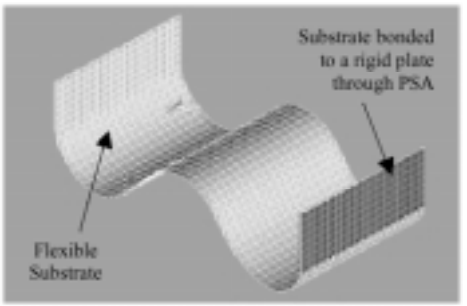

Figure 3. The Finite Element Analysis (FEA) model.

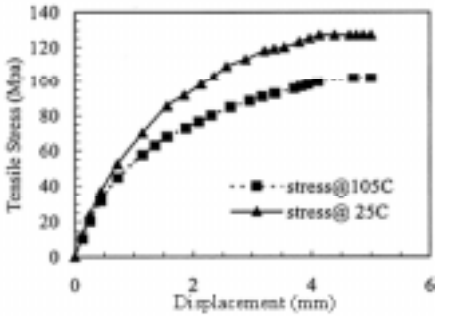

Figure 4. The FEA data: tensile strain versus displacement.

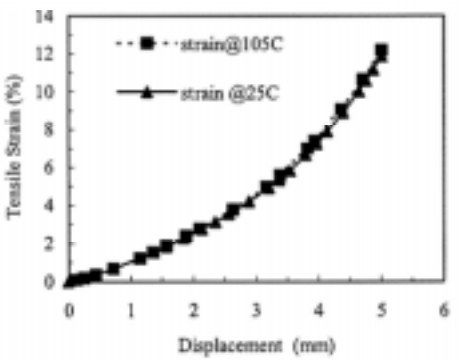

Figure 5. The FEA data: tensile stress versus displacement.

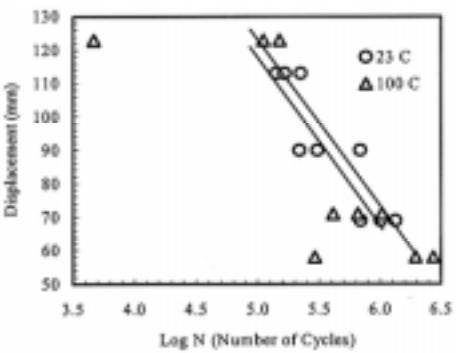

Figure 6. S-N diagram for material system A constructed based on experimental and FEA data.

The actual construction of the flexible substrate consists of several components, and the FEA model is simplified. The substrate is represented by a thin layer of equivalent thickness and effective material property. The mechanical behavior of the flexible substrates is studied in a separate publication [11]. The stress-strain curves measured at various temperatures can be found in that reference.

Shown in Figure 4 and Figure 5 are the numerical results from FEA. They present tensile strain and tensile stress as a function of displacement load, respectively. Both graphs indicate nonlinearity as displacement increases. These results have been used to generate the conventional *S-N* fatigue curves. Figure 6 provides the typical *S-N* curve for a material system A, on the basis of experimental data and FEA results. As described above, three data

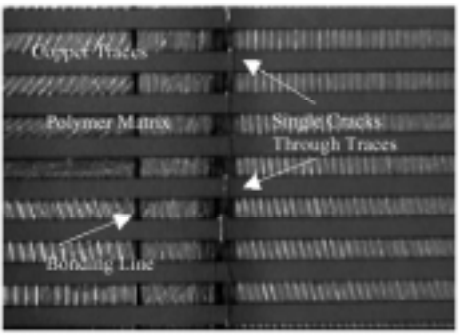

Figure 7. Digital image of fracture surface of material system A under ambient temperature (23°C).

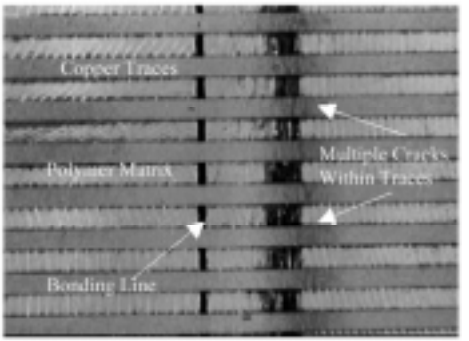

Figure 8. Digital image of fracture surface of material system A under elevated temperature (100°C).

points (minimum, maximum and average fatigue lifetime) are given for each loading condition to reflect the scatter of fatigue performance of various traces subjected to the same testing conditions. Clear decline in the fatigue performance of this material system is observed with the increase of stresses. It is worthy noting that the fatigue data obtained in this work results from a non-zero mean process. The non-zero stresses are induced by the substrate forming. Analysis of the effect of mean stress is to be reported elsewhere.

In contrast with to our expectations, the higher temperature increases fatigue lifetime of material system A. This is clearly seen in Figure 2. It may be related to the softening mechanisms within the polymer matrix caused by elevated temperatures, which increase adhesiveness of circuit traces, slows down brittle failure process and increases fatigue lifetime. Final comparative analysis of all three material systems is unfinished at the present.

Finite Element Analysis showed that within the applied loading range, the temperature effect on stress is significant while it is negligible for strain. For a displacement controlled failure process, rising temperature is likely to delay the failure time.

Fracture analysis reveals the potential causes of the effect via direct observation of the failure modes. Figure 7 is the image of fracture surface in material system *A* under room temperature. Well-developed and aligned across the width cracks can be seen on the bonding line of the sample setup. Optical microscopy of various samples confirmed the fact that all the cracks were initiated within the copper circuit traces. However, it had been found that in few cases crack occurred along the metal/polymer interface. Simultaneous single cracks could be observed in various traces without interconnection at the initial stages. However, on the final stages of failure process they are all connected with each other through the polymer matrix. Temperature affects the failure mechanism in this particular material structure. Figure 8 presents the fracture surface of copper circuit traces (system A) under elevated

temperature (100°C). An array of multiple cracks within the same copper trace could be observed. It can be attributed to softer polymer matrixes or adhesives due to higher temperature, which reduce "rigid" movements of the flex and diminish to some extent brittle crack initiation within the copper traces. Therefore, there is an apparent variation in the failure mechanism with temperature.

CONCLUSIONS AND FUTURE WORK

High cycle fatigue resistance of copper circuit traces in FPC (three material systems) as a function of frequency, displacement and temperature has been analyzed. Novel testing procedure has been designed and new experimental setup has been developed. Comparative analysis of selected materials based on fatigue lifetime evaluation is in progress. Failure analysis has been performed and failure mechanisms have been identified for material system A. Typical *S-N* curves for the same material system are constructed. Wider frequency and temperature range are being analyzed at present. Reliability assessment is also being performed via statistical analysis of the data.

ACKNOWLEDGEMENTS

The financial support of Automotive and Industrial Electronics Group, Motorola Inc. is gratefully acknowledged. Assistance in manufacturing and assembling of the continuity monitor from Mr. Ted Lester and his invaluable inputs to this project are greatly appreciated.

REFERENCES

1 P. Viswanadham and P. Singh, "**Failure Modes and Mechanisms in Electronic Packages**", *Chapman and Hall*, New York, 1998.
2 Proceedings: Eighth Electronic Materials and Processing, Ed. S. Rao, ASM International, 1994.
3 J. C. Cluley, "**Electronic Equipment Reliability**", *John Wiley and Sons*, New York, 1974.
4 S. W. Hinch, "**Handbook of Surface Mount Technology**", *Longman Scientific & Technical*, New York, 1988.
5 W. Sikonowiz, "**Designing and Creating Printed Circuits**", *Hayden Book Company, Inc*., New Jersey, 1981.
6 G. L. Ginsberg, "**Printed Circuits Design**", *McGraw-Hill, Inc*., 1991.
7 C. F. Coombs, Jr., "**Printed Circuits Handbook**", 3 rd edition, *McGraw-Hill, Inc.*, 1988.
8 D. Steinberg, "**Vibration Analysis for Electronic Equipment**", Second Edition, *John Wiley and Sons*, New York, 1988.
9 "**Handbook of Flexible Circuits**", Ed. K. Gilleo, *Van Norstrand Reinhold*, 1992.
10 S. Gurley, "**Flexible Circuits: Design and Applications**", *Marcel Dekker, Inc*., New York and Basel, 1984.
11 M. Lu, Z. Qian, S. Liu, R. Li and L. Poglitsch, "Thermo-Mechanical Behaviors of Flexible Substrates", *J. Electronic Packaging*, in press, 1999.

Fatigue Behavior of Discontinuous Glass Fiber Reinforced Polypropylene

Mustafa Sezer
Arcelik A.S., Istanbul, Turkey
Ahmet Aran
Istanbul Technical University, Istanbul, Turkey

INTRODUCTION

Fatigue is known as the failure of materials under the cyclic loads below their yield strengths. Although there is a tendency about the increasing use of plastics in mechanical components, the designers can't find enough data to predict the fatigue performance of plastics as it is for metals. Since the polymers are not rigid in their neat polymer state, they can be reinforced with long and short glass, carbon, aramid, polyester, or other fibers to increase the stiffness, stability, heat conductivity and fatigue resistance. Injection molding process is the most convenient to add fillers and reinforcements to the polymers.

Wohler (S-N) curves are the conventional method to investigate the fatigue behavior of polymers. S-N curves have been used to investigate the tensile and flexural fatigue behaviors of long and short glass fiber reinforced polymers.[1-4] Fatigue crack propagation (FCP) method is also very popular method to determine the fatigue behavior of glass fiber reinforced polypropylenes.[5-8]

In this study, fatigue behavior and failure of 30 wt% short glass fiber reinforced chemically coupled and uncoupled polypropylenes were investigated. One aim of this study is to create design data for the above mentioned materials in the design of dynamic components. To increase the knowledge capacity about the failure and fatigue mechanism of the materials is the second aim of the study.

EXPERIMENTAL

In this study 30 wt% chemically coupled (CCPP) and uncoupled (UCPP) glass fiber reinforced polypropylene's supplied by TARGOR were used (GC30H251 and GF30H152). Maleic anhydride grafting were used in CCPP to increase the bonding property between the fibers and the matrix polymer. The polypropylenes used as matrices were homopolymer and isotactic. The average diameter of glass fibers were 10 microns. A separate study was per-

formed with 500 fibers before and after the injection to evaluate the fiber breakage during the injection molding. According to the results, the glass fiber lengths have lowered to 15% during the injection.[9,10] Materials properties used in the studies are given in Table 1.

Table 1 Physical and mechanical properties of materials used in the tests

	CCPP (GC30H251)	UCPP (GF30H152)
Tensile strength (23°C, 5 mm/min)	67 MPa	41 MPa
Young's modulus (23°C, 1 mm/min)	6645 MPa	5773 MPa
Elongation at break (23°C, 5 mm/min)	2.2%	1.3%
Izod impact strength (23°C, notched)	10 kJ/m^2	4 kJ/m^2
Heat deflection temperature /A (1.8 MPa)	151°C	95°C

ISO 527 Type I tensile test specimens were used for static and dynamic tests. The width of parallel portion and measuring length were 10 and 50 mm respectively. A semi-automatic injection molding machine, MANUMOLD 77/30, was used to produce test specimens. Injection molding parameters were determined according to ISO 294, ISO 1873-2 and the proposals of material manufacturer. Detailed injection molding parameters were in reference.[11] Test specimens were conditioned under 23°C and 50% humidity according to ISO 291 in HERAUS HC 4030 circulated climatic cabin before the static and cyclic tests.

An Instron electromechanical test machine was used for the static tensile tests. For the fatigue tests, an MTS servo-controlled hydraulic test machine was used. The load ratio (minimum load/maximum load) was chosen as 0.1 and sinusoidal wave form was used in the fatigue tests.

To check the reliability of taking the stroke as specimen elongation, some dummy cyclic tests were done with marked tensile test specimens. During these tests, stroke and elongation data were saved by both MTS and "Kodak Ektapro Motion Analysis (KEMA)" systems. Then elongation of marking traces were measured on the monitor of KEMA system by help of frozen and magnified images. Very satisfied results were obtained.

Wohler curves were constructed with tensile test specimens which were subjected to fatigue tests at different stress coefficients. Fatigue tests conditions were same with above and each point on the curve is the average of 5 experiments.

Frequency is an important parameter to occur the hysteretic failure or mixed mode (hysteretic heating and mechanical failure) failure on the test specimens. Pilot tests which were performed at 1 Hz, 5 Hz and 10 Hz, to determine the effect of test frequency on heat-

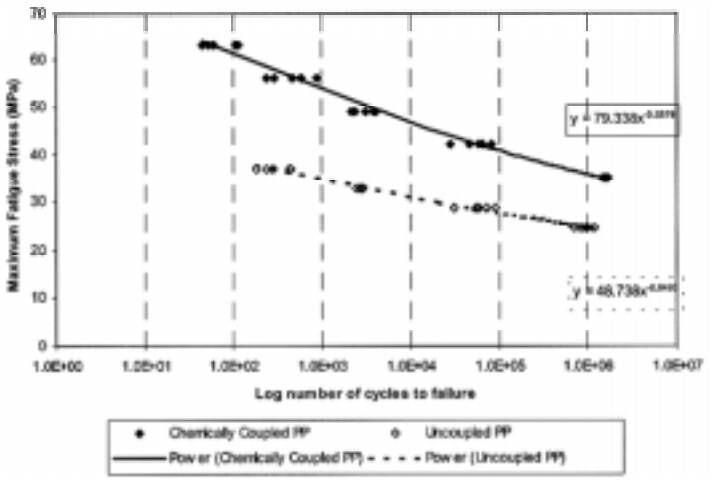

Figure 1. The variation of maximum fatigue stress of CCPP and UCPP with the number of fatigue cycles (Wohler curves).

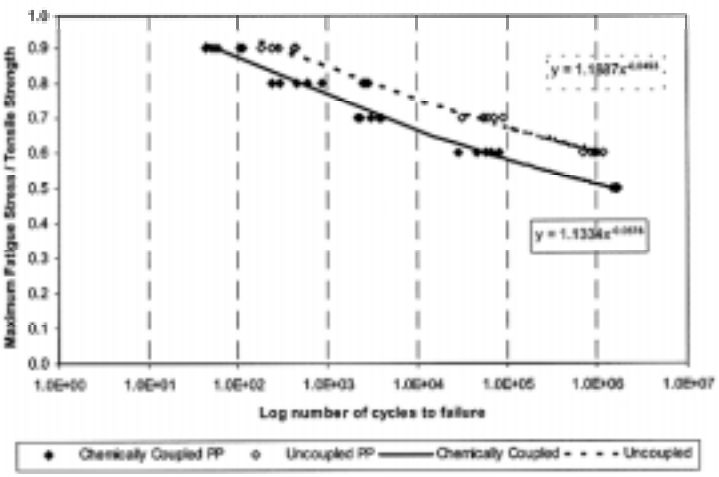

Figure 2. The variation of normalized of maximum fatigue stress of CCPP and UCPP with the number of fatigue cycles (normalized Wohler curves).

ing. Temperatures were observed first by the contactless infrared thermometer and then by surface type thermocouples. Temperature was nearly constant for 1 Hz and early failures were observed for 5 Hz and 10 Hz.[11]

After tensile tests were applied to fatigued and unfatigued test specimens, scanning electron microscope (SEM) investigations were performed.

RESULTS AND DISCUSSION

WOHLER (S-N) DIAGRAMS

Fatigue test results are shown in Figure 1 and Figure 2 as Wohler curves. The fatigue strength of CCPP is much more than UCPP (Figure 1) as expected. But normalized fatigue strength (ratio of upper fatigue stress level to tensile strength) of UCPP is higher than the CCPP (Figure 2). The deterioration trends of normalized fatigue strengths are similar. No endurance limits were determined for both CCPP and UCPP as seen in diagrams (Figure 1 and Figure 2). Fluctuations of fatigue test results for both materials are within acceptable limits and results can be used in engineering calculation. According to Wohler curves, improving fiber-matrix bonding does not only improve the tensile

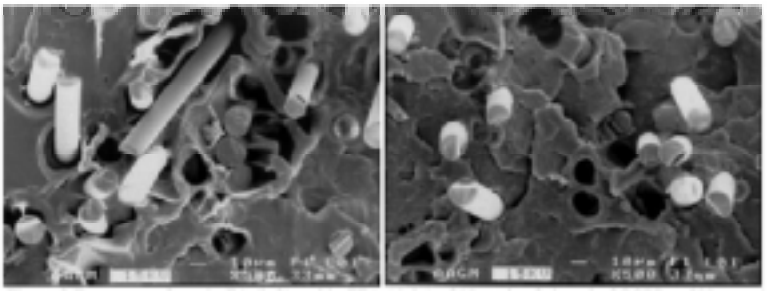

Figure 3. Fracture surfaces in FA (left) and in FFA (right) of 10 cycles fatigued of CCPP at 500 magnifications.

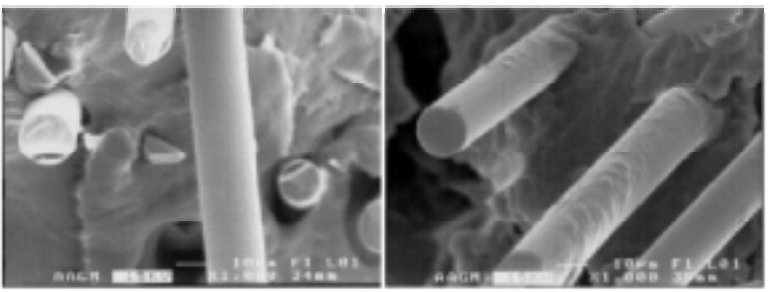

Figure 4. Fiber surfaces in FA (left) and in FFA (right) of naturally fatigued of CCPP at 1000 magnifications.

strength but the fatigue strength also (Figure 1). In despite of improved bonding results, normalized fatigue strength of CCPP is lower than UCPP (Figure 2) because of the debonding process.

MICROSCOPIC INVESTIGATIONS

Tensile tests are performed on unfatigued and fatigued specimens and their fracture surfaces were investigated. Although only brittle fracture was observed on the fracture surface of unfatigued CCPP, the crack surface of 10 cycles fatigued specimen shows 2 different regions (Figure 3). In the first region (FA), holes were observed around the fibers in the matrix and since fiber-matrix bonding does not exist anymore, the matrix has started to bear the load (Figure 3). Ductile type fracture was observed in this region (FA). The other region called as FFA has brittle fracture surface (Figure 3). Here, matrix and fibers have still good bonding. FFA type fracture was observed at the fiber ends, where the bond of matrix and fibers exists (Figure 4) and some matrix particles were seen on the surface of pulled-out fibers.

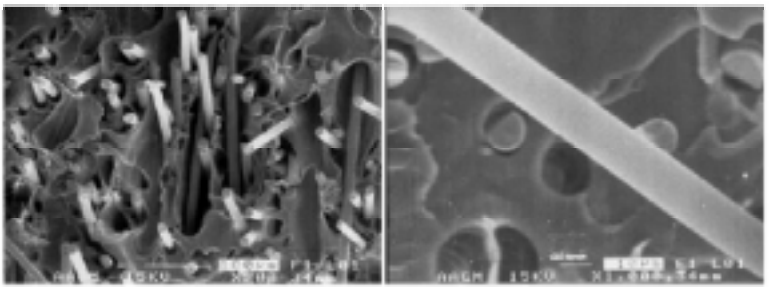

Figure 5. Fracture surfaces in elastic deformation portion of unfatigued UCPP at 200 magnifications (left) and fiber surface in FFA of naturally fatigued of UCPP at 1000 magnifications (right).

On the fracture surfaces of unfatigued UCPP specimens, big deterioration were observed at the fiber-matrix bondings and ductile fracture was observed on the matrix (Figure 5). On the contrary, we have not seen matrix particles on the surface of pulled-out fibers in FFA for UCPP (Figure 5).

FATIGUE FAILURE MECHANISM

On the crack surfaces of fatigued CCPP specimens, brittle fracture observed only in one region. Totally brittle fracture (no ductile fracture) was observed on the fracture surface of unfatigued specimens. When the brittle fracture occurred, the matrix particles were seen on surfaces of the pulled-out fibers. As a result, if some ductile fracture on the matrix and no adhering matrix particles on surfaces of the pulled-out fibers were observed, we can conclude that some fatigue loading have been applied to the specimen.

At the fiber ends local stresses are high and poor bonding may occur. During fatigue loading, failure starts as debonding at the fiber ends and develops along the interface. Since failure propagates along the interfaces no adhering matrix particles were seen on surfaces of the pulled-out fibers. This type of failure results as a ductile failure on the matrix. In tensile test, matrix cracks in a brittle manner since there is no time to occur a failure at the interfaces. Failure occurs at the matrix near the fibers instead of interfaces and these matrix particles will be seen on the pulled-out fibers.

In UCPP, ductile fracture was also observed on the fracture surface of unfatigued specimens. Besides, no adhering matrix particles on surfaces of the pulled-out fibers in FFA were observed because of the poor bonding in UCPP.

During the microscopic study, we have also noticed that the debonding effect of the alternating stresses (the region where ductile fracture is observed) propagates as “failure front”.

According to the above observations, the occurrence of a fatigue failure can be summarized as follows:

1. Failure starts as voids at the fiber ends. The fiber ends are the potential stress concentration areas because both they are discontinuous regions for stress lines and they don't have enough sizing.
2. Fiber-matrix debonding propagates along the fibers with cyclic movements.
3. Because of the debonding process, matrix starts to bear the load and ductile deformation is observed.
4. Composite replies with more strain to the applied load for the reason of the debonding fibers. This case results with the new fiber-matrix debondings.
5. The voids continues to grow and merge into cracked areas. The cracked areas develops to form a big main crack.
6. For the reason of the debonding fibers, load bearing capacity of composite to become lower. After the FA grows to the extend that loads cannot be carried by the remaining cross-section and material fails under tensile stresses in a brittle manner.[3]

CONCLUSIONS

1. Fatigue failure mechanisms of CCPP and UCPP are nearly the same, except that UCPP has weaker fiber-matrix interface and crack propagates faster than CCPP.
2. During the microscopic study we notify that fatigue crack propagates as a "failure front".
3. Fluctuations in the fatigue test results for both materials are within acceptable limits and the results can be used it in engineering calculation confidently. Fatigue data can be shown as S-N curves and both materials do not show any endurance limits.

ACKNOWLEDGMENTS

The authors wish to thank for the support of Arcelik A.S. The authors also wish to thank to Research and Development Center for giving a permission to use the test capability and thank to Mr. Turgay GONUL to help us in SEM studies.

REFERENCES

1 Grove, D., Kim, H., Cooper, D. and Ellis C., Longitudinal Fatigue Behavior of Long and Short Glass Reinforced, Injection Moldable, Polypropylene Composites, 26th International SAMPE Conference, pp. 281-295, October 17-20, (1994).

2 Grove, D. and Kim, H., Fatigue Behavior of Long and Short Glass Reinforced Thermoplastics, Advances in Automotive Plastic Components and Technology SP-1099, SAE Inc., pp. 77-83, February, (1995).

3 Grove, D. A. and Kim, H. C., Effect of Constituents on the Fatigue Behavior of Long Fiber Reinforced Thermoplastics, ANTEC'95, SPE, (1995).

4 Dally, J. W. and Carrillo, D. H., Fatigue Behavior of Glass-Fiber Fortified Thermoplastics, *Polym. Eng. Sc*i., Vol. **9**, No. 6, November, (1969).
5 Carling, M. J., Manson, J. A., Hertzberg, R. W. and Attalla, G., Effects of Fiber Orientation and Interfacial Adhesion on Fatigue Crack Propagation in Short-Glass-Fiber Reinforced Polypropylene Composites, ANTEC'85, SPE, (1985).
6 Karger-Kocsis, J., Freidrich, K. and Bailey R. S., Fatigue Crack Propagation in Short and Long Glass Fiber Reinforced Injection-Molded Polypropylene Composites, *Adv. Composite Mater.*, Vol. **1**, No. 2, pp. 103-121, (1991).
7 Karger-Kocsis, J., Freidrich, K. and Bailey R. S., Fatigue and Failure Behavior of Short and Long Glass Fiber Reinforced Injection-Molded Polypropylene, *Sci. Eng. Composite Mater.*, Vol. **2**, No. 1, pp. 50-67, (1991).
8 Harmia, T., Fatigue Behavior of Neat and Long Glass Fiber (LGF) Reinforced Blends of Nylon 66 and Isotactic PP, *Polym. Composites*, Vol. **17**, No. 6, pp. 926-936, (1996).
9 Sezer, M., ABN-082 "Reinforced Polypropylene", Research and Development Center of Arcelik A.S., Internal Research Report, (1996).
10 Sezer, M., ABR-056 "Design and Manufacturing Properties of Reinforced Polypropylene", Research and Development Center of Arcelik A.S., Internal Research Report, (1997).
11 Sezer, M., Fatigue Behavior of Discontinuous Glass Fiber Reinforced Polypropylene, Ph. D. Thesis, Istanbul Technical University, (1999).

Ductile Failure and Delayed Necking in Polyethylene

W. Zhou, D. Chen, Y. Shulkin, A. Chudnovsky
Department of Civil & Materials Engineering, University of Illinois at Chicago, Chicago, Illinois 60607, USA
N. Jivraj, K. Sehanobish, S. Wu
The Dow Chemical Company, Freeport, Texas 77541, USA

INTRODUCTION

The time dependent micromechanisms of deformation and fracture has been observed in many engineering materials. Extensive studies of time dependent strain localization in form of shear bands and crazes of semicrystalline and amorphous polymers have been published.[1,2] Creep yielding in polymers is well known to occur at high strain.[3-5] The same phenomenon is also recognized in nonpolymeric materials, for example, a change in mechanism from ductile failure of ligaments between voids to transgranular and intergranular microcracking in chromium steel under creep has been reported.[6]

The neck formation and propagation constitutes the yielding process in a PE tensile drawing experiment. The engineering yield stress, σ_y, is taken as the first maximum of the engineering stress. The engineering draw stress, σ_{dr}, is defined as an essentially constant engineering stress under which the neck propagates. With the increasing application of polyethylene as a durable material, its fracture behavior has received considerable attention. It is generally accepted that all the modes of fracture in polyethylene are intimately associated with the development of cavitation, drawing and crazing or material as a precursor to fracture.

In the present work, the time dependent (delayed) necking is investigated under displacement (ramp) and load (creep) control conditions. The results obtained from these experiments are employed to characterize a similar phenomenon, the ductile failure of PE pipes.

Ductile failure of a PE pipe manifests itself in appearance of a bulge on the pipe wall (ballooning). The bulge is extended in the longitudinal direction of the pipe and accompanied by significant thinning of the wall. The study of PE ductile failure under sustained hydrostatic pressure tests (e.g., ASTM 2837 and ISO/TR 9080) is a very involving and time consuming process. In addition, the experiments with pipes can often require large amount of material that may not be available at an early stage of material development. Thus a

methodology of material durability characterization based on tensile specimens testing is of practical and economic importance.

EXPERIMENTAL DETAILS

The ASTM D-638 Type-IV tensile specimens were prepared from a European PE 100 HDPE grade 32 mm diameter pipes. The specimens, with the gage length and the cross section of 30 mm and 2 mm x 7 mm. respectively, and grip lengths of 40 mm, were cut in machine direction. All tests were conducted at ambient temperature (23°C). Tensile ramp tests were performed on an Instron Testing Machine at various strain rates. Long-term creep tests were conducted on a tensile creep station equipped with a LVDT. For the tensile creep tests, several stress levels were chosen above and below the draw stress σ_{dr} observed in the ramp test with strain rate 3.3×10^{3} s^{-1}. Initial loading rate in the load application on the creep station is about 3×10^{-2} MPa s^{-1}. The rate of creep strain was taken as a creep rate at the steady stage of the process.

THE RESULTS OF TENSION TESTS

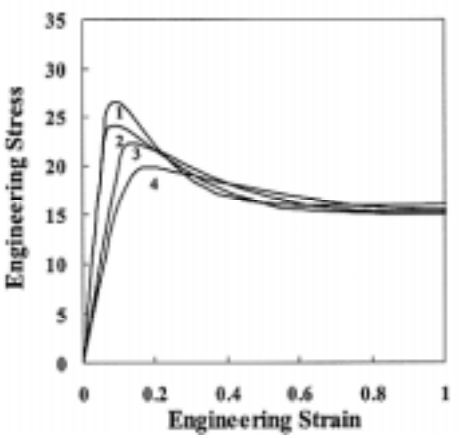

Figure 1. Stress-strain diagrams of PE 100 HDPE ramp test at strain rates. 1 - $\dot{\varepsilon}$ = 0.33 s^{-1}, 2 - $\dot{\varepsilon}$ = 0.033 s^{-1}, 3 - $\dot{\varepsilon}$ = 0.0033 s^{-1}, 4 - $\dot{\varepsilon}$ = 0.00033 s^{-1}.

The engineering yield stress, σ_y, is associated with significant shear band formation.[7-9] A two-stage process of onset of yielding has been reported.[10] The first stage is the formation of thin microshear band packets spreading over a narrow region prior to the second stage of a large scale shearing of that narrow region resulting in a macroshear band formation. The second stage of this process produces most of the shear strain in the shear band. On further strain, the shear bands coalesce to form a well-defined neck whose boundaries propagate under essentially constant draw stress, σ_{dr}.

Figure 1 shows the engineering stress–engineering strain curves at various strain rates under displacement control conditions (ramp tests). The strain rate dependence of yielding stress σ_y and drawing stress σ_{dr} are presented in Figure 2. Decrease in strain rate from 3.3×10^{-1} s^{-1} to 3.3×10^{-3} s^{-1}, i.e., by two orders of magnitude, resulting in decrease of σ_y by about 30%. The draw stress σ_{dr} is less dependent on the strain rate, i.e., as a change in the strain rate from 3.3×10^{-1} s^{-1} to 3.3×10^{-3} s^{-1}, resulting in only 10% decrease in σ_{dr}. Thus, the differ-

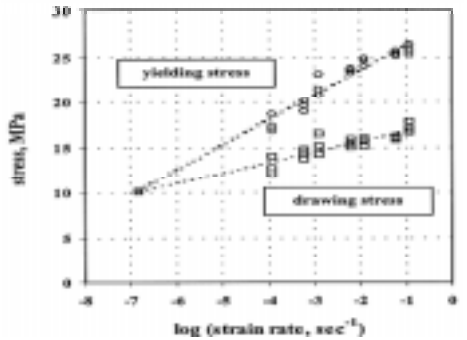

Figure 2. Ramp test. Dependence of yielding and drawing on strain rate.

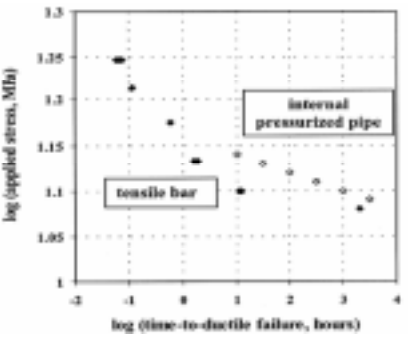

Figure 3. Time-to-necking and -to-ductile failure vs. applied stress (HDPE: BG10050).

ence between the yield stress and draw stress, $\sigma_y - \sigma_{dr}$, is reduced with the decrease of strain rate. If this tendency is extrapolated further, one can identify a certain strain rate, at which the value of yield stress would coincide with that of draw stress. This common value of σ_y and σ_{dr} is called the characteristic stress and denoted by σ_0. According to the data shown on Figure 2, the characteristic stress σ_0 of HDPE is about 10 MPa and corresponds to the ramp test with strain rate $\dot{\varepsilon}_0 = 10^{-7}$ s^{-1}. It suggests that the yielding at this strain rate occurs with no overshooting.

In the creep tests, at loads above the characteristic stress σ_0, progression of a homogeneous stretching was observed until a sudden neck formation at time t_n called the time to (delayed) necking. The relation between time to necking and applied stress are shown in Figure 3 by filled points. It is instructive to compare these data with stress vs. time in ductile failure of HDPE pipes at high stresses.[12]

INTERNALLY PRESSURIZED PIPE VS. TENSILE BAR

In a thin-walled pipe of large length under internal pressure p, the hoop, axial and radial stresses (Figure 4a), σ_θ, σ_s, and σ_r are related to each other as $\sigma_s = \nu\sigma_\theta$, $\sigma_r = -p$ (<0), and $|\sigma_r| << \sigma_\theta$ with ν being Poisson's ratio. If one disregards the small component σ_r, the state of the pipe becomes plane strain, $\varepsilon_s = 0$. As seen from Figure 4b, the pipe experiences yielding (ductile failure) in the hoop direction. Unlike the pipe, the prismatic bar cut out from the pipe in its axial direction and subjected to axial tension (Figure 5a) has only one non-zero stress component σ_s. In this connection two questions arise. The first is about the difference in failure behavior of the pipe material with respect to hoop θ and axial *s* directions. In other words, would failure tests in axial direction be valid to characterize the failure in hoop direction? Comparison of the ductile failure behavior in s-direction (tests of the

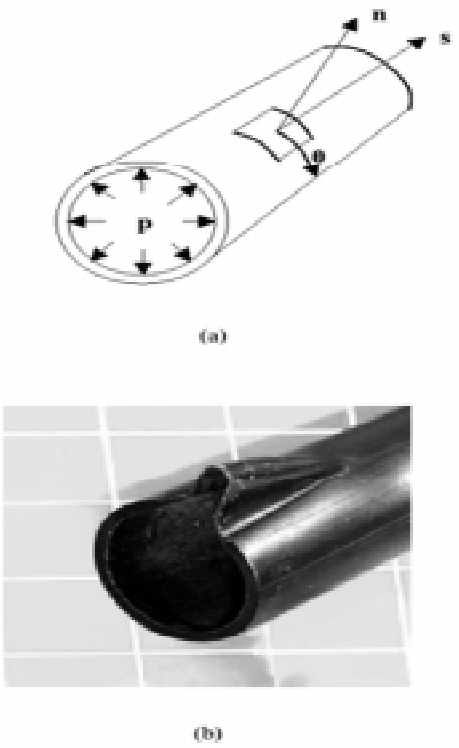

Figure 4. Internally pressurized pipe: (a) hoop ϑ –. axial *s*- and normal n-directions; (b) Ductile failure (PE 100 HDPE).

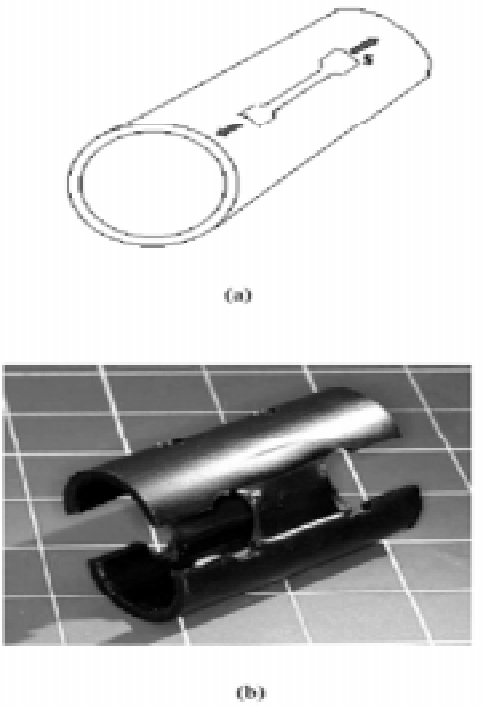

Figure 5. Isotropy of pipe material with respect to ductile failure: (a) test in axial s-direction; (b) test in hoop ϑ -direction.

tensile specimen, see Figure 5a) and that in θ -direction (tests of the pipe, Figure 5b) shows that within an experimental error the pipe material is isotropic with respect to necking.

The second question is related to the fact that the tensile bar is in an uniaxial stress state, whereas the pipe is in biaxial or even triaxial stress state. Is it correct to judge the pipe failure based on experiments with the tensile bars? Let the yielding point of the pipe material be determined by the Tresca or von Mises criterion. For the pipe, one has $\sigma_1 = \sigma_0$, $\sigma_2 = \nu\sigma_0$ and $\sigma_3 = -p$ with $|\sigma_3| << \sigma_1$. If the first criterion is accepted, $\sigma_y = \sigma_1 - \sigma_3 = \sigma_0$ where σ_y is the yield stress at uniaxial tension, i.e., σ_s and σ_r do not influence the yielding point. For the second criterion, $\sigma_y \approx \sigma_0\sqrt{1-\nu+\nu^2}$, and since the material is almost incompressible ($\nu \approx 0.45$), $\sigma_y \approx 0.87\sigma_0$. Thus, the bar is supposed to be equivalent to the pipe if the

stress of the bar is 13% higher than that of the pipe. However, the correspondence of the bar and pipe needs to be further investigated.

The correlation between time to ductile failure and time to necking is seen from Figure 2. The open circles represent the ISO TR 9080 Hoop Stress Testing datapoints of ductile failure for a European PE 100 pipe grade HDPE. The above data also allow the estimation of the stress σ_c of ductile-brittle transition at 20^{o}C. The approximate value of σ_c is 10 MPa, i.e., about the same as the characteristic stress σ_0 (see Figure 2). The equality of σ_c and σ_0 is not a mere coincidence. Indeed, the yielding in PE at stress σ_y is directly associated with ductile failure, and results from breaking up of the lamellae crystal stacks as well as individual crystal, resulting in largely non-recoverable morphological rearrangements.[13] The brittle fracture is associated with a craze formation triggered by cavitation within the amorphous phase at stress level of σ_{dr} and below.[9,11] Thus, when $\sigma_y \cong \sigma_{dr} \cong \sigma_0$ both ductile and brittle mechanisms of failure may occur at the same time and which one of them actually takes place is controlled by chance. It results in a large scatter of time to failure at stress about σ_0 and corresponds to the transition in fracture mechanisms from ductile above σ_0 to brittle below that value.

CONCLUSIONS

The estimation of the time to ductile failure on the basis of the test for delayed necking is in a good agreement with the direct observations of PE pipes ductile failure in the sustained hydrostatic pressure test performed in accordance with ISO/TR 9080. A recent advances in an understanding of the delayed necking phenomenon, specifically σ_y and σ_{dr} dependence on strain rate in the ramp tests, led to identification of the characteristic stress σ_0 that corresponds to the ductile-brittle transition in PE fracture mechanisms. This stress, when placed on the stress-lifetime diagram, connects the ductile failure line with the brittle one. Thus, this paper, in combination with previously reported studies on brittle fracture, as well work being presented at this conference,[14] offer a basis for an accelerated testing for PE pipes failure for the entire range of stresses that encompass both ductile and brittle modes of PE failure.

REFERENCES

1 Crist, B. Structure and Properties of Polymers, Vol 12 of "**Materials Science and Technology**", Thomas, E.L., *VCH Publishing* 1993.
2 Andrews E. H. **Fracture in polymers**, *American Elsevier*, New York, 1968.
3 Turner, S. in '**The Physics of Glassy Polymers**' (Ed. R. N. Haward), *Wiley & Sons*, New York, 1973, p. 250.
4 Ender, D. H. and Andrews, R. D., *J. Appl. Phys*., 1955, **36**, 3057.
5 Brady, T. E. and Yeh, G. S. Y., *J. Appl. Phys.*, 1971, **42**, 4622.
6 Gooch, D., *J. Metals Science*, 1982, **16**, 79.

7 Ma, M., Vijayan, K., Hiltner, A., Baer, E. and Im, J.: Shear yielding modes of polycarbonate. *J. Mater. Sci*., **24**: 2687 -2696, 1989.
8 Kim, A., Garrett, L. V., Bosnyak, C. P. and Chudnovsky, A., Modeling the process zone kinetics of polycarbonate, *J. Applied Polymer Sci*., **49**: 877-883, 1993.
9 Stokes, V. K. and Bushko, W. C.: Use of plastics and plastic composites: Materials and Mechanics Issues. V. K. Stokes, ed.: 1- 21, MD-vol 46. American Society of Mechanical Engineers, New York, 1993.
10 Matsuoka, S.: **Relaxation phenomena in polymers**. *Hanser Publishers*, New York, Ch. 3, 1992.
11 Zhou, W., Chudnovsky, A., Sehanobish, K. and Bosnyak, C.P.: Understanding of the time-dependent fracture phenomena of polycarbonate. Proc. of the 3 rd International Symposium on Risk, Economy and Safety, Failure Minimization and Analysis, Pilanesberg, South Africa, July 6-10, 1998, page 139-150.
12 Williams, J. G, **Fracture Mechanics of Polymers**, *Ellis Horwood Ltd*., 1984.
13 Zhou, W., Chudnovsky, A., Sehanobish, K. and Bosnyak, C.P. SPE'99, 1999.
14 Fan, J., Chen, D., Shulkin, Y., Chudnovsky, A., Jivraj, N., Sehanobish, K., " Application of the Crack Growth Layer Model for Understanding of the Correlation between Lifetime and Creep Behavior in Polyethylene", SPE ANTEC 2000.